Published in final edited form as:
Dev Cell. 2012 May 15; 22(5): 940–951. doi:10.1016/j.devcel.2012.04.009.

IFT25 Links the Signal-Dependent Movement of Hedgehog Components to Intraflagellar Transport

Brian T. Keady, **Rajeev Samtani**[2], **Kimimasa Tobita**[2], **Maiko Tsuchya**[2], **Jovenal T. San Agustin**, **John A. Follit**, **Julie A. Jonassen**[1], **Ramiah Subramanian**[2], **Cecilia W. Lo**[2], and **Gregory J. Pazour**[‡]

Program in Molecular Medicine, University of Massachusetts Medical School, Biotech II, Suite 213, 373 Plantation Street, Worcester, MA 01605

[1]Department of Microbiology and Physiological Systems, University of Massachusetts Medical School, 55 Lake Avenue North, Worcester MA 01655

[2]Department of Developmental Biology, University of Pittsburgh, 8111 Rangos Research Center, 530 45th Street, Pittsburgh, PA 15201

Abstract

The intraflagellar transport (IFT) system is required for building primary cilia, sensory organelles that cells use to respond to their environment. IFT particles are composed of about 20 proteins and these proteins are highly conserved across ciliated species. IFT25, however, is absent from some ciliated organisms suggesting it may have a unique role distinct from ciliogenesis. Here, we generate an *Ift25* null mouse and show that IFT25 is not required for ciliary assembly but is required for proper Hedgehog signaling, which in mammals occurs within cilia. Mutant mice die at birth with multiple phenotypes indicative of Hedgehog signaling dysfunction. Cilia lacking IFT25 have defects in the signal-dependent transport of multiple Hedgehog components including Patched-1, Smoothened, and Gli2 and fail to activate the pathway upon stimulation. Thus, IFT function is not restricted to building cilia where signaling occurs, but also plays a separable role in signal transduction events.

Keywords

intraflagellar transport; Hedgehog signaling; cilia

Introduction

Primary cilia extend from the surface of most types of vertebrate cells and function as sensory organelles. In vertebrates, but curiously not in invertebrates, the cilium is the organizing center for Hedgehog signaling, an essential pathway required for development (Corbit et al., 2005; Huangfu and Anderson, 2005). In the absence of Sonic Hedgehog (Shh) ligand, the Patched-1 (Ptch1) receptor resides in the ciliary membrane. Upon stimulation by Shh ligand, Ptch1 exits the cilium and consequently triggers the ciliary accumulation of the Smoothened (Smo) receptor (Rohatgi et al., 2007). Gli transcription factors, which are the

[‡]Corresponding Author: Telephone: 508 856 8078, Fax: 508 856 2950, gregory.pazour@umassmed.edu.

downstream effectors, localize to cilia, accumulate at ciliary tips after pathway activation, and translocate to the nucleus to regulate gene expression (Haycraft et al., 2005; Kim et al., 2009; Tukachinsky et al., 2010). During development, Shh signaling plays key roles in the development of the limbs, brain, heart and most other organ systems and it is likely that alteration of the Shh pathway by ciliary defects underlies many of the pathologies seen in the ciliary diseases or ciliopathies. However, in spite of its importance to mammalian development, the mechanism that vertebrates use to compartmentalize Shh signaling within the cilium remains unknown.

Cilia are assembled by intraflagellar transport (IFT), a process that moves large complexes called IFT particles from the cell body into and along the ciliary microtubules. The particles are carried to the flagellar tip using kinesin-2 motors and then back to the cell body using cytoplasmic dynein 2 (Rosenbaum and Witman, 2002). The IFT particles are composed of more than twenty subunits organized into two subcomplexes called A and B (Cole et al., 1998; Follit et al., 2009). In mouse, mutations in complex B subunits and in the kinesin motor typically result in a loss of cilia and an attenuated Shh pathway (Houde et al., 2006; Huangfu and Anderson, 2005; Liu et al., 2005; Ocbina and Anderson, 2008). Most mutations in the retrograde IFT motor dynein 2 produce short stumpy cilia and also yield an attenuated Shh pathway (Huangfu and Anderson, 2005; May et al., 2005). Mutations in complex A have produced varying results with either stumpy cilia and enhanced Shh signaling (*Ift139*, $Ift122^{sopb}$) or failed cilia assembly and weakened Shh signaling ($Ift122^{Med1\Delta 1-3}$) (Cortellino et al., 2009; Qin et al., 2011; Tran et al., 2008).

IFT proteins are highly conserved throughout ciliated species. Two intriguing exceptions to this conservation are the complex B proteins IFT27 (NM_025931) and IFT25 (NM_028394), which are conserved in vertebrates but not found in *C. elegans* and *Drosophila.* IFT27 is a member of the small G protein family and is most closely related to the Rab subfamily (Qin et al., 2007). IFT25 was originally identified as a small heat shock protein (Bellyei et al., 2007) but its membership in the heat shock family was recently called into question (Bhogaraju et al., 2011). Work in mouse (Follit et al., 2009) and *Chlamydomonas* (Lechtreck et al., 2009; Wang et al., 2009) strongly support its role as an IFT complex B subunit. Furthermore, recent structural analysis revealed that IFT25 and IFT27 reside in a binary complex (Bhogaraju et al., 2011).

The observation that IFT25 and IFT27 are not conserved in some ciliated organisms such as *C. elegans* and *Drosophila* but are conserved in mammals suggests that these two proteins may have distinct roles outside of the conventional IFT-B role in ciliary assembly. To further elucidate the function of IFT25, we generated an *Ift25* null mutant mouse. All other mouse IFT complex B null mutants fail to assemble cilia properly and die mid-gestation. In contrast, *Ift25* null mutants retained the ability to ciliate and survived through gestation. The mutants die at birth with severe heart defects and also display phenotypes indicative of aberrant Shh signaling. Cell culture experiments and *in vivo* analysis indicate that IFT25 is required for the export of Smo and Ptch1 receptors out of the cilium and the accumulation of Gli2 at the ciliary tip in response to activation of the Shh pathway. We propose that IFT25 is not required for ciliary assembly but rather for the dynamic transport of Shh signaling molecules within the cilium.

Experimental Procedures

Additional methods can be found in Supplemental Experimental Procedures

Mouse Breeding—*Ift25*-targeted ES cell line 2900042B11Rik was obtained from the EUCOMM project and injected into C57Bl/6J albino blastocysts to generate chimeric animals. Chimeric mice were mated to C57Bl/6J albino mice (B6(Cg)-Tyr^{c-2J}/J, Jax 000058)

or to C57Bl/6J mice (Jax 000664). Germline deletion was carried out using a C57Bl/6 congenic PrmCre (O'Gorman et al., 1997). Genotyping was carried out as described in Figure S1. All mouse work was carried out at UMMS and was approved by the UMMS IACUC.

Cell Culture—Primary mouse embryonic fibroblasts (MEF) from e14 embryos were cultured in 90% DMEM (4.5 g/L glucose), 10% fetal bovine serum, 1 mM sodium pyruvate, 0.1 mM NEAA, 10 mM HEPES, 100 U/ml penicillin, and 100 μg/ml streptomycin (all from Gibco-Invitrogen). Early passage cells (<4 passages) were used for analysis. For Shh and SAG experiments, MEFs were plated at near confluent densities and serum starved (same culture medium described above but with 0.25% FBS) for 48 hr prior to treatment to allow ciliation. SAG (Calbiochem) was used at 400nM and Shh (R&D Systems) was used at 2μg/ml.

Immunofluorescence Microscopy, Histology, and Electron Microscopy—Cells for immunofluorescence microscopy were grown, fixed, and stained as described (Follit et al., 2006) except that the paraformaldehyde fixation time was reduced to 15 min. For some antibodies, an antigen retrieval step of 0.05% SDS in PBS for 5 minutes was used prior to the blocking step (Brown et al., 1996). For H&E staining and trachea immunofluorescence, tissues were fixed overnight at 4°C with 4% paraformaldehyde in PBS, paraffin embedded, and processed as previously described (Jonassen et al., 2008). For neural tube immunostaining, embryos were fixed in 4% paraformaldehyde in PBS for 1 hr at 4°C, rinsed in PBS, equilibrated overnight at 4°C in PBS with 30% sucrose, and embedded in OCT Tissue Freezing Medium (Triangle Biomedical Sciences). Cryosections (10 μm) were blocked for one hour at room temperature in TBS containing 5% goat serum and 0.1% Triton and then incubated in primary antibody overnight at 4°C.

Primary antibodies used included acetylated tubulin (611-B1, Sigma), beta-tubulin (B-5-1-2, Sigma), MmIFT20, MmIFT52, MmIFT57, MmIFT88 (Pazour et al., 2002), MmIFT25 (Proteintech), MmIFT140 (Jonassen et al., 2012), Gli1 (V812, Cell Signaling), Gli3 (AF3690, R&D), beta actin (13E5; Cell Signaling), Gli2 (gift of J. Eggenschwiler, Princeton Univ), Smo, and Ptch1 (gifts of R. Rohatgi, Stanford Univ.). Nkx2.2, FoxA2, Pax7, and Pax6 antibodies were from DSHB (University of Iowa). Anti-MmIFT27 was made by expressing the mouse protein in bacteria as a maltose binding protein fusion and injecting into rabbits (Figure S3). IFT antibodies were affinity purified against the same fragment expressed as a glutathione S-transferase fusion. Further microscopy details are provided in Supplemental Experimental Procedures.

Skeletal preparations were performed with Alcian Blue (Sigma) and Alizarin red (Sigma) as previously described (Tsumaki et al., 1999) with slight modifications (0.03% Alizarin red in 1% KOH).

For quantification of Gli2 at ciliary tips, the average Gli2 fluorescence intensity within a defined circular area of 320 pixels at the distal end of each axoneme was measured using the measurement tools of Openlab. Gli2 quantitation data was compiled from measurements of 50 cilia from each of 3 wild type cell lines and 3 mutant cell lines.

Protein and mRNA Analysis—For determining IFT protein levels, MEFs were lysed directly into denaturing loading buffer. Western blots were developed by chemiluminescence (Super Signal West Dura, Pierce Thermo) and imaged using a LAS-3000 imaging system (Fujifilm).

Isolation of mRNA and quantitative mRNA analysis was performed as previously described (Jonassen et al., 2008). Primers are listed in Supplemental Experimental Procedures.

Episcopic Fluorescence Image Capture (EFIC) Histology and MicroCT Imaging—EFIC and MicroCT imaging were performed as previously described (Rosenthal et al., 2004; Tobita et al., 2010). Detailed information is included in Supplemental Experimental Procedures.

Data analysis

All quantitations are presented as means ± SD and were compared between mutant and wild type mice with unpaired *t* tests using GraphPad software. Differences between groups were considered statistically significant if $p < 0.05$. Statistical significance is denoted with asterisks (*p=0.01–0.05; **p=0.001-0.01;***p<0.001).

Results

Ift25 mutants die at birth with multi-organ structural birth defects

To characterize the function of IFT25, we generated a mutant mouse using EUCOMM ES cells (Skarnes et al., 2011). The original ES cell line contained a splice acceptor, a promoterless β-galactosidase-neomycin resistance gene fusion and a LoxP recombination site inserted into intron 2 and an additional LoxP site inserted into intron 3 (Figure S1). This cell line was injected into blastocysts and used to create the $Ift25^{neo}$ allele. The $Ift25^{neo}$ allele was converted to the $Ift25^{null1}$ allele by a germ line Cre. The null1 allele retained the splice acceptor and β-galactosidase-neomycin resistance gene fusion insertion but lacked exon 3. In both cases, the splice acceptor and fusion gene are expected to capture the upstream exons and disrupt splicing and or translation of the downstream exons. We examined both $Ift25^{null1}$ and $Ift25^{neo}$ mutant animals but found no differences between the two genotypes (Figure 1, 2). We were unable to detect IFT25 protein by western blot from either allele (Figure 3E and data not shown) and the mRNA levels of the 3′ exons were at background levels by quantitative PCR (Figure 1B) strongly suggesting that these are null alleles.

In stark contrast to the mid gestational lethality observed when other IFT B genes are deleted in the mouse, $Ift25^{null1}$ and $Ift25^{neo}$ mutants are born live but none survive past the day of birth (Figure 1A). At birth the *Ift25* mutant animals are smaller than littermates and are cyanotic (Figure 1C). To understand the pathology leading to the neonatal lethality, we examined embryos the day prior to birth (e18). At e18 the mutant embryos were alive but had a number of abnormalities. In addition to a slight growth restriction (Figure 2D), they frequently showed omphaloceles (23/29 $Ift25^{neo/neo}$ mutants and 21/40 $Ift25^{null1/null1}$) (Figure 1D) and often had polydactyly (6/29 for $Ift25^{neo/neo}$ mutants and 6/40 for $Ift25^{null1/null1}$) with a preaxial digit duplication (Figure 1Ec). Mutants also displayed other skeletal malformations such as micrognathia, cleft palate (Figure 1Ea, 1Ed), and malalignment of the sternal vertebrae (Figure 1Eb). The kidneys did not show any sign of cyst formation at e18 (data not shown).

Cyanosis is often caused by heart and lung defects. Histological analysis indicated that cellular development of the *Ift25* mutant lungs was not greatly affected and at most, only slight hypoplasia was detected. However, a subset of the animals (2/6 for $Ift25^{neo/neo}$ mutants and 6/15 for $Ift25^{null1/null1}$) had a left pulmonary isomerism where a single lobe was present on both sides rather than the normal arrangement of four lobes on the right and one on the left (Figure 2B). Necropsy indicated that in many cases, the rib cage was small and impinged on the lungs, deforming their surface, findings consistent with a short-rib

phenotype. Quantitative analysis using microCT imaging showed a reduction in the chest cross sectional area. However, mutant animals were smaller and the reduction in chest size was proportional to the crown to rump length. In contrast, the heart size was not reduced proportionally, and it is likely that a normal size heart in a smaller chest cavity caused the compression of the lungs (Figure 2C). Besides the pulmonary isomerism, no other evidence of left-right asymmetry defects was observed (0/6 $Ift25^{neo/neo}$ mutants and 0/14 $Ift25^{null1/null1}$embryos showed alterations in orientation of the heart or position of stomach and spleen).

The *Ift25* mutant animals also displayed severe structural heart defects including ventricular septal defects (VSD) and outflow tract malalignment defects comprising of overriding aorta or double outlet right ventricle (Figure 2Ab). In addition, *Ift25* mutants had severe endocardial cushion defects, also referred to as atrioventricular septal defects (AVSD) (Figure 2Aa). Instead of two AV orifices with mitral and tricuspid valves separating the left atrium and ventricles versus right atrium and ventricles, *Ift25* mutants have a single orifice with common AV valves. In some mutants, the AV orifice is located more in favor of the right ventricle, referred to as an unbalanced AVSD. These defects are associated with a common atrium due to complete failure in formation of the septum primum and septum secondum (Figure 2Aa). The severity of these congenital heart defects, particularly the common atrium and AVSD are not compatible with postnatal survival and this is likely the cause of the neonatal lethality seen in the mutant animals.

IFT25 is not required for cilia assembly

The ability of the *Ift25* mutants to survive past the point at which most IFT complex B mutants die suggests that they would not completely lack cilia. Indeed, examination of e18 lung sections showed normal numbers and lengths of cilia on the epithelial cells of the bronchi (Figure 3A) and TEM analysis of trachea cilia revealed no major ultrastructural differences (Figure 3B). Furthermore, no significant differences were seen in either the percentage of ciliated cells or the ciliary lengths in mouse embryonic fibroblast (MEF) cultures (Figure 3D). Strikingly, the assembled cilia on *Ift25* mutant cells contained normal distributions of IFT88 and IFT140 but were devoid of IFT27 (Figure 3C, S3) suggesting that IFT27 may be specifically affected by the *Ift25* mutation. To examine how the lack of IFT25 affected IFT27 and other IFT proteins, extracts derived from MEF cell lines were examined by western blotting. As expected, IFT25 was undetectable in homozygous *Ift25* mutant cells. Although most of the IFT subunits we tested (IFT88, 57, 20, 140) were not significantly affected by the loss of IFT25, IFT27 was strongly depleted (Figure 3E). These data indicate that the stability of IFT27 is dependent on IFT25 and that both proteins are likely dispensable for cilia assembly. We also did not detect significant mitotic defects in *Ift25* mutant cells (data not shown), suggesting that mammalian IFT25 is likely not required for cell cycle control.

Ift25 mutants have Hedgehog signaling defects

Mouse mutants that fail to assemble cilia typically exhibit aberrant Shh signaling. Interestingly, although the *Ift25* mutant embryos form cilia normally, they still display phenotypes of Shh signaling defects, including polydactyly, cleft palate, lung isomerisms and ventricular septal defects (Goddeeris et al., 2008; Johnson, 1967; McMahon et al., 2003; Mo et al., 1997; Tsukui et al., 1999) (Figure 1, 2). This observation suggests that the cilia on *Ift25* mutants may have defects in Shh signaling. However, these phenotypes may be caused by defects in other signaling pathways. To more directly test the Shh pathway, we used an *in vitro* assay to measure the upregulation of *Gli1* and *Ptch1* in response to pathway activation by the Smo agonist SAG. Treatment of wild type cells with SAG activates the pathway at Smo, stimulating the downstream events to elevate *Gli1* and *Ptch1* expression (Humke et al.,

2010). As previously reported, cells from ciliary assembly mutants like *Ift88*^{Tg737Rpw} assemble reduced numbers of cilia (Figure 4C) and display weakened Shh signaling (indicated by decreased upregulation of Gli1 and Ptch1 in response to SAG compared to controls) (Figure 4B) (Haycraft et al., 2005). In contrast, the *Ift25* mutant cells assembled normal numbers of cilia (Figure 4C) yet still showed a weakened Shh signaling response (Figure 4A). Therefore, although both *Ift25* and *Ift88* mutants have a weakened Shh signaling response, the underlying causes are likely quite different.

The expression pattern of transcription factors within the developing neural tube is often used as a readout of Shh signaling. The notochord resides ventral to the neural tube and produces high levels of Shh. This establishes a gradient across the neural tube with high Shh on the ventral side and low Shh on the dorsal side. In response to high levels of Shh, the most ventral cells differentiate into the floor plate and become a secondary source of Shh that reinforces the gradient. The Shh gradient within the neural tube effects which target transcription factor genes will be expressed (Goetz et al., 2009). For example, Pax6 is normally expressed in the dorsal region of the neural tube but is repressed at the ventral pole due to the high level of Shh signaling in this region. Similarly, Olig2 is repressed by high levels of Shh signaling, but requires moderate levels of Shh signaling for expression so this transcription factor is found in a zone at the middle of the neural tube. Mouse mutants that fail to properly assemble cilia (e.g. mice with mutations in most complex B genes) exhibit aberrant expansion of dorsal markers into ventral regions of the neural tube (Ko et al., 2009). This is interpreted as weakened Shh signaling. Similar to what is seen in cilia-defective embryos, *Ift25* mutants had an aberrant expansion of the Pax6 and Olig2 domains towards the ventral pole of the caudal neural tube (Figure 5A,B) suggesting that the *Ift25* mutation also causes weakened Shh signaling. However, this is complicated in both our *Ift25* mutant and in other cilia defective mutants (Ko et al., 2009) as the floor plate cells in these lines fail to become secondary sources of Shh (Figure 5B) and so it is likely that the gradient is less established. Despite these defects at e9.5, the neural tube patterning appeared to be largely corrected by e10.5 (Figure S5), suggesting a significant diminution but not a complete block of Shh signaling in the *Ift25* mutant neural tube at e.9.5.

Patterning of limb is also dependent on Shh signaling and the finding of polydactyly in the hindlimbs of *Ift25* mutant animals suggested that Shh signaling might be altered. During limb development, the Shh gradient affects the processing of Gli3 into the cleaved repressor form and cilia-defective mutants typically show increased amounts of Gli3 full length protein. Likewise, the *Ift25* mutants also displayed significantly increased levels of full length Gli3 in the hindlimbs (Figure 5C) suggesting that *Ift25* is required for the processing of this transcription factor.

*Ift*25 mutants are defective in signal-dependent redistribution of Hedgehog components

The weakened Shh signaling seen in other loss of cilia mutants could be due to the cell's inability to concentrate Shh signaling components into its signaling compartment (the cilium). However, the *Ift25* mutants also have weakened Shh signaling despite the presence of normal cilia. This suggests that the dynamic localizations of Shh signaling components within cilia might be perturbed in *Ift25* mutants. To test this, we monitored the redistribution of Gli2, Smo and Ptch1 in MEFs in response to activation of the pathway. In the basal state, Gli2 is normally found in the cytoplasm with a small enrichment at the ciliary tip. Upon stimulation, Gli2 rapidly accumulates at the ciliary tip so that by 30 min a detectable increase is observed; after 24 hrs there is a large pool at this site and Gli2 is now observed in the nucleus (Figure 6A, B). In *Ift25* mutant cells, the small pool is present at the ciliary tip in the basal state, but there is greatly diminished accumulation of Gli2 at both the ciliary tips and the nucleus after stimulation of the pathway (Figure 6A, B). A similar phenotype was found in the embryonic neural tube. Normally, Gli2 is highly enriched at the tip of cilia in

the neural tube. In the *Ift25* mutant embryos, the ciliary level was reduced and the remaining Gli2 was more evenly distributed along the ciliary shaft (Figure 6C). In wild type cells under basal conditions, Ptch1 is found in the cilium but Smo is not, and upon activation of the pathway, ciliary Ptch1 decreases and Smo increases (Figure 7A). In *Ift25* mutant MEFs, Ptch1 is localized to the cilia under unstimulated conditions as expected, but is not exported from the cilium after pathway activation. Although ciliary Smo levels increase after activation of the pathway, Smo is abnormally present in the cilia of unstimulated *Ift25* mutant MEFs (Figure 7A). This accumulation of ciliary Smo and Ptch1 was even more striking *in vivo*. Embryonic tissues that are normally Shh responsive, such as the paraxial mesoderm, have broad cell body distributions of Smo and Ptch1 and relatively low levels within cilia. In contrast, Smo and Ptch1 are highly enriched in the cilia of *Ift25* mutants (Figure 7B, C, S7). Since low levels of Smo and Ptch1 are thought to dynamically enter and exit the cilium under unstimulated conditions (Kim et al., 2009; Ocbina et al., 2011) their abnormal ciliary accumulation in *Ift25* mutants suggest defects in the ability of these cilia to export Smo and Ptch1 in response to extracellular cues.

Discussion

IFT25 is not required for ciliary assembly

The function of the IFT particle in the transport of ciliary components and the assembly of cilia is well established but little is known about the functions of individual subunits of the particle. The high degree of conservation across eukaryotes of the ~20 IFT particle proteins suggests that each subunit has important and unique functions. However, analysis of individual subunits has been hampered by the fact that strong alleles of most IFT genes disrupt the particle and cause ciliary assembly defects. A defective ciliary assembly phenotype precludes the ability to attribute specific functions to individual IFT proteins (as opposed to a function of IFT in general) and precludes the ability to study ciliary trafficking of signaling components.

In this work, we generated an *Ift25* knockout mouse. In contrast to all previously characterized null alleles of IFT complex B genes in mouse, *Ift25* is not required for ciliary assembly. Our analysis indicates that cilia are present in the mutants in normal numbers and with normal structure both in cultured fibroblasts and throughout the embryo. However, cilia of the *Ift25* mutants contained no detectable IFT27. This finding is interesting in light of the observation that these two proteins are direct binding partners of each other and may exist as a heterodimer outside of the IFT particle (Bhogaraju et al., 2011). Thus, we cannot rule out the possibility that some of the phenotypes in the *Ift25* mutant might be partially due to a combined loss of IFT25/IFT27. No *Ift27* mouse mutants have been published so it is unclear whether *Ift27* mutants would phenocopy the *Ift25* mutants. The only known perturbations of *Ift27* are *Chlamydomonas* RNAi knockdown lines, which suggested that IFT27 was critical for cytokinesis and cell cycle control (Qin et al., 2007). We did not observe cytokinesis defects in our *Ift25* mutant fibroblasts and the mitotic index was the same in mutant and control MEFs suggesting that cell cycle is not greatly altered by the loss of mammalian IFT25/27.

Ift25 mutant mice have Hedgehog phenotypes

The finding that IFT25 is not required for ciliary assembly is consistent with the fact that *Ift25* was lost from some invertebrates, like *Caenorhabditis* and *Drosophila* that still assemble cilia. However, IFT25 is not dispensable in organisms that retained the gene as *Ift25* mutant mice died shortly after birth with a constellation of phenotypes reminiscent of Shh signaling defects. These phenotypes include polydactyly, cleft palate, lung isomerisms and structural heart defects (Figure 1, 2) Although lung and heart defects are also found in

mouse mutants with defects in left-right axis determination due to motile cilia defects, the phenotypes in the *Ift25* mutant are more consistent with Shh signaling defects than motile ciliary defects. For example, motile cilia defects often result in *situs inversus* or reversal of the lung pattern (Tan et al., 2007), but the *Ift25* mutants show duplication of the left lung, a phenotype nearly identical to that seen in the Shh mutant mouse (Tsukui et al., 1999). Likewise an AVSD similar to one in the *Ift25* mutant heart is seen in the Shh mutant and when *Smo* is specifically deleted in the dorsal mesenchyme protrusion, an extracardiac tissue that migrates into the heart to form the atrial septum (Goddeeris et al., 2008; Hildreth et al., 2009). In contrast, motile cilia defects cause left-right phenotypes like heterotaxy and *situs inversus* (Tan et al., 2007) not seen in the *Ift25* mutant hearts.

Observations from numerous groups have led to the idea that the cilium functions in a seemingly paradoxical manner to either activate or repress the Shh pathway, depending on the cellular context (Goetz et al., 2009; May et al., 2005). In the neural tube and agonist stimulated MEFs, loss of a cilium typically impedes the upregulation of Gli activators (such as Gli1) thus causing a weakened signaling output. In the limb bud, however, loss of the cilium typically reduces the processing of Gli3 into Gli3-R and causes polydactyly, which is thought to be the result of increased pathway activity. This difference is probably related to the observation that the cilium is needed for the Gli transcription factors to be modified by proteolysis and phosphorylation to stabilize them and convert them from inactive to active activator or repressor forms (Tuson et al., 2011). Despite the presence of normal cilia, *Ift25* mutants displayed Shh phenotypes that are similar to loss of cilia mutants (i.e. weakened upregulation of Gli1 activator in MEFs and increased levels of Gli3-FL in limb buds). These data suggest that IFT25 functions downstream of ciliary assembly, but like the cilium, is critical for production of the appropriate forms of Gli transcription factors in various tissues. There is much left to understand about the mechanics of the Shh pathway, but it appears that Ptch1 plays a dual role in transmitting a signal to Smo when the pathway is activated and a negative role in inhibiting Smo when the pathway is inactive. The mechanism by which Ptch1 activates Smo is not known but is proposed to be through small molecule intermediates (Wang et al., 2007) and is likely to involve the phosphorylation of Smo (Chen et al., 2011). Likewise the repressive role of Ptch1 is not clear, but Ptch1 may sequester ciliary Smo keeping it inactive. In *Ift25* mutants, there is an increase in both Ptch1 and Smo in the cilium and the pathway is attenuated. This may simply be due to the level of Ptch1 in the cilium being adequate to sequester all of the Smo in the cilium or may be due to a more complicated mechanism. For example, Gli2 is not trafficked to the ciliary tip in response to pathway activation. If Gli transcription factors are actively transported by IFT25, the failure to transport them to the tip would cause an attenuation of the pathway regardless of what is happening to Ptch1 and Smo.

The proposed role of IFT25 in Shh signaling fits well with the conservation of the gene in vertebrates and its loss in *Drosophila* and *Caenorhabditis*. While Shh signaling is cilia-dependent in vertebrates, this pathway does not appear to be present in *Caenorhabditis* and is cilia-independent in *Drosophila* (Wilson and Stainier, 2010). However, the fact that IFT25 is conserved in *Chlamydomonas*, which does not appear to use Shh signaling since core components are missing from its genome, suggests that it also had an ancestral role in other signaling pathways prior to the evolution of Shh signaling. For example, the mating response in *Chlamydomonas* involves dynamic movement of signaling components in cilia that are reminiscent of Shh signaling (Wang et al., 2006) and perhaps these are dependent upon IFT25.

IFT25 is required for the dynamic movements of Hedgehog components in cilia

The role of the cilium and IFT in vertebrate Shh signaling is well established but the fundamental question of whether IFT plays a direct role in the signaling cascade or whether

it functions only to assemble the cilium where the components are organized remains unanswered. Null or strong hypomorphic mutations in IFT complex B components and the anterograde motor *Kif3a* typically cause a complete failure of the cilium to assemble and result in attenuated Shh signaling (Ko et al., 2009). In these cases it is not possible to distinguish a direct role for IFT in Shh signaling from its role in ciliary assembly. IFT complex A mutations are more complicated. A null allele of *Ift139* resulted in short and stumpy cilia with overactive Shh signaling (Tran et al., 2008). IFT complex A has often been described as being primarily involved in retrograde transport and it was proposed that the defects in retrograde transport caused an accumulation of Shh components in the cilia and this resulted in an overactive pathway. However, alleles of the retrograde dynein motor also accumulate Shh components in cilia but result in attenuation of the pathway rather than its activation (May et al., 2005; Ocbina and Anderson, 2008). The phenotype of *Ift25* is distinct from all of the previous mouse mutations in IFT components. The *Ift25* mutants have some phenotypes similar to IFT-A mutants (ciliary accumulation of Shh components) yet also have some phenotypes similar to IFT-B mutants (attenuated Shh pathway). These data indicate that the view that complex B plays predominantly a role in anterograde transport while complex A plays predominantly a role in retrograde transport is overly simplistic. It is more likely that individual subunits within the two complexes have specific functions in maintaining the particle structure, in connecting the particle to the motors and in coupling the cargos to the particle. For example, the lack of IFT25 in the ciliated organisms *Drosophila*an d *Caenorhabditis* coupled with the lack of ciliary structural defects in *Ift25*mutant mice suggest that IFT25 is not integral for basic “housekeeping” functions of the IFT particle such as axoneme assembly. Instead, IFT25 is more likely to function in signaling dependent transport of specific cargo within the cilium. Our finding that Ptch1 and Smo accumulate in the *Ift25* mutant cilia suggests that IFT25 functions to couple the dynamic movement of these proteins to the IFT system. Our work is consistent with a model whereby the ciliary export, but not import, of Ptch1 and Smo requires IFT25 (Figure 7D). In the absence of Shh ligand, Ptch1 does not get exported by IFT, but Smo is actively removed from the cilium. Upon stimulation of the pathway, the inhibitor (Ptch1) gets removed from the cilium and the activator (Smo) accumulates there. However, when IFT25 is missing, Ptch1 remains ectopically trapped in the cilium and thus keeps the pathway in an attenuated state (Figure 7D).

Clinical Implications

Despite the multitude of known ciliopathy genes, *IFT80* is the only complex B gene found mutated in human patients thus far (Beales et al., 2007). This dearth of IFT complex B mutations in human diseases is likely explained by the fact that loss of cilia in mice causes mid-gestational lethality around the time of heartbeat initiation (~e10.5), which in humans would correlate with an early term miscarriage. The fact that *Ift25* mutant mice survive gestation suggests that IFT25 is a good candidate for human ciliopathies. Interestingly, the IFT25 mouse phenotype is quite similar to the clinical manifestations of Jeune Asphyxiating Dystrophy which combines skeletal abnormalities such as polydactyly, with lung hypoplasia. Furthermore, Ellis-van Creveld syndrome and McKusick-Kaufman syndromes present with similar skeletal abnormalities in addition to cardiac disorders such as septal defects and a common atrium (Hills et al., 2011), which are all observed in the *Ift25* mutant mouse.

Conclusions

Our finding that IFT25 is not required for ciliary assembly but does cause major defects in Shh signaling allows us, to demonstrate that IFT participates in Shh signaling and is not just involved in ciliary assembly. Since all previous IFT mutants had at minimum, moderate defects in ciliary assembly it has been argued that IFT does not play a direct role in Shh

signaling but is only required for producing the proper ciliary architecture for signaling to occur. Our data demonstrates that IFT plays a larger role as mutations in *Ift25* do not produce any changes in ciliary abundance nor cause any detectable structural defects or abnormal accumulations of IFT proteins yet the Shh components fail to undergo the dynamic movements that normally occur during Shh signaling. Thus, IFT25 couples Shh components to IFT to allow for the dynamic movements that are needed for signaling.

Supplementary Material

Refer to Web version on PubMed Central for supplementary material.

Acknowledgments

We thank Drs. S. Jones (Transgenic Mouse Core) G. Hendricks (Electron Microscopy Core) and P. Furcinitti (Digital Imaging Core) for assistance during this work and Dr. R. Bloodgood for carefully reading the manuscript. We also thank Dr. P. Odgren for use of his bright field microscope, and Drs. J. Eggenschwiler (Princeton Univ) and R. Rohatgi (Stanford Univ) for reagents. This work was supported by the National Institutes of Health (GM060992 to GJP) and (5U01HL098180 to CWL). Core resources supported by the Diabetes Endocrinology Research Center grant DK32520 were also used.

Abbreviations

Shh	Sonic Hedgehog
Smo	Smoothened
Ptch1	Patched 1
H&E	hematoxylin and eosin
IFT	intraflagellar transport
SD	standard deviation
MEF	mouse embryonic fibroblast
TEM	transmission electron microscopy
e	embryonic
p	postnatal
EFIC	episcopic fluorescence image capture
AVSD	atrioventricular septal defect
AV	atrioventricular
VSD	ventricular septal defect

References

Beales PL, Bland E, Tobin JL, Bacchelli C, Tuysuz B, Hill J, Rix S, Pearson CG, Kai M, Hartley J, et al. IFT80, which encodes a conserved intraflagellar transport protein, is mutated in Jeune asphyxiating thoracic dystrophy. Nat Genet. 2007; 39:727–729. [PubMed: 17468754]

Bellyei S, Szigeti A, Pozsgai E, Boronkai A, Gomori E, Hocsak E, Farkas R, Sumegi B, Gallyas F Jr. Preventing apoptotic cell death by a novel small heat shock protein. Eur J Cell Biol. 2007; 86:161–171. [PubMed: 17275951]

Bhogaraju S, Taschner M, Morawetz M, Basquin C, Lorentzen E. Crystal structure of the intraflagellar transport complex 25/27. Embo J. 2011; 30:1907–1918. [PubMed: 21505417]

Brown D, Lydon J, McLaughlin M, Stuart-Tilley A, Tyszkowski R, Alper S. Antigen retrieval in cryostat tissue sections and cultured cells by treatment with sodium dodecyl sulfate (SDS). Histochem Cell Biol. 1996; 105:261–267. [PubMed: 9072183]

Chen Y, Sasai N, Ma G, Yue T, Jia J, Briscoe J, Jiang J. Sonic Hedgehog Dependent Phosphorylation by CK1alpha and GRK2 Is Required for Ciliary Accumulation and Activation of Smoothened. PLoS Biol. 2011; 9:e1001083. [PubMed: 21695114]

Cole DG, Diener DR, Himelblau AL, Beech PL, Fuster JC, Rosenbaum JL. Chlamydomonas kinesin-II-dependent intraflagellar transport (IFT): IFT particles contain proteins required for ciliary assembly in Caenorhabditis elegans sensory neurons. J Cell Biol. 1998; 141:993–1008. [PubMed: 9585417]

Corbit KC, Aanstad P, Singla V, Norman AR, Stainier DY, Reiter JF. Vertebrate Smoothened functions at the primary cilium. Nature. 2005; 437:1018–1021. [PubMed: 16136078]

Cortellino S, Wang C, Wang B, Bassi MR, Caretti E, Champeval D, Calmont A, Jarnik M, Burch J, Zaret KS, et al. Defective ciliogenesis, embryonic lethality and severe impairment of the Sonic Hedgehog pathway caused by inactivation of the mouse complex A intraflagellar transport gene Ift122/Wdr10, partially overlapping with the DNA repair gene Med1/Mbd4. Dev Biol. 2009; 325:225–237. [PubMed: 19000668]

Follit JA, Tuft RA, Fogarty KE, Pazour GJ. The intraflagellar transport protein IFT20 is associated with the Golgi complex and is required for cilia assembly. Mol Biol Cell. 2006; 17:3781–3792. [PubMed: 16775004]

Follit JA, Xu F, Keady BT, Pazour GJ. Characterization of mouse IFT complex B. Cell Motil Cytoskeleton. 2009

Goddeeris MM, Rho S, Petiet A, Davenport CL, Johnson GA, Meyers EN, Klingensmith J. Intracardiac septation requires hedgehog-dependent cellular contributions from outside the heart. Development. 2008; 135:1887–1895. [PubMed: 18441277]

Goetz SC, Ocbina PJ, Anderson KV. The primary cilium as a Hedgehog signal transduction machine. Methods Cell Biol. 2009; 94:199–222. [PubMed: 20362092]

Haycraft CJ, Banizs B, Aydin-Son Y, Zhang Q, Michaud EJ, Yoder BK. Gli2 and Gli3 localize to cilia and require the intraflagellar transport protein polaris for processing and function. PLoS Genet. 2005; 1:e53. [PubMed: 16254602]

Hildreth V, Webb S, Chaudhry B, Peat JD, Phillips HM, Brown N, Anderson RH, Henderson DJ. Left cardiac isomerism in the Sonic hedgehog null mouse. J Anat. 2009; 214:894–904. [PubMed: 19538633]

Hills CB, Kochilas L, Schimmenti LA, Moller JH. Ellis-van Creveld Syndrome and Congenital Heart Defects: Presentation of an Additional 32 Cases. Pediatr Cardiol. 2011

Houde C, Dickinson RJ, Houtzager VM, Cullum R, Montpetit R, Metzler M, Simpson EM, Roy S, Hayden MR, Hoodless PA, Nicholson DW. Hippi is essential for node cilia assembly and Sonic hedgehog signaling. Dev Biol. 2006; 300:523–533. [PubMed: 17027958]

Huangfu D, Anderson KV. Cilia and Hedgehog responsiveness in the mouse. Proc Natl Acad Sci U S A. 2005; 102:11325–11330. [PubMed: 16061793]

Humke EW, Dorn KV, Milenkovic L, Scott MP, Rohatgi R. The output of Hedgehog signaling is controlled by the dynamic association between Suppressor of Fused and the Gli proteins. Genes Dev. 2010; 24:670–682. [PubMed: 20360384]

Johnson DR. Extra-toes: anew mutant gene causing multiple abnormalities in the mouse. J Embryol Exp Morphol. 1967; 17:543–581. [PubMed: 6049666]

Jonassen JA, San Agustin J, Follit JA, Pazour GJ. Deletion of IFT20 in the mouse kidney causes misorientation of the mitotic spindle and cystic kidney disease. J Cell Biol. 2008; 183:377–384. [PubMed: 18981227]

Jonassen JA, SanAgustin J, Baker SP, Pazour GJ. Disruption of IFT complex A causes cystic kidneys without mitotic spindle misorientation. J Am Soc Nephrol. 2012:ASN.2011080829.

Kim J, Kato M, Beachy PA. Gli2 trafficking links Hedgehog-dependent activation of Smoothened in the primary cilium to transcriptional activation in the nucleus. Proc Natl Acad Sci U S A. 2009; 106:21666–21671. [PubMed: 19996169]

Ko HW, Liu A, Eggenschwiler JT. Analysis of hedgehog signaling in mouse intraflagellar transport mutants. Methods Cell Biol. 2009; 93:347–369. [PubMed: 20409825]

Lechtreck KF, Luro S, Awata J, Witman GB. HA-tagging of putative flagellar proteins in Chlamydomonas reinhardtii identifies a novel protein of intraflagellar transport complex B. Cell Motil Cytoskeleton. 2009; 66:469–482. [PubMed: 19382199]

Liu A, Wang B, Niswander LA. Mouse intraflagellar transport proteins regulate both the activator and repressor functions of Gli transcription factors. Development. 2005; 132:3103–3111. [PubMed: 15930098]

May SR, Ashique AM, Karlen M, Wang B, Shen Y, Zarbalis K, Reiter J, Ericson J, Peterson AS. Loss of the retrograde motor for IFT disrupts localization of Smo to cilia and prevents the expression of both activator and repressor functions of Gli. Dev Biol. 2005; 287:378–389. [PubMed: 16229832]

McMahon AP, Ingham PW, Tabin CJ. Developmental roles and clinical significance of hedgehog signaling. Curr Top Dev Biol. 2003; 53:1–114. [PubMed: 12509125]

Mo R, Freer AM, Zinyk DL, Crackower MA, Michaud J, Heng HH, Chik KW, Shi XM, Tsui LC, Cheng SH, et al. Specific and redundant functions of Gli2 and Gli3 zinc finger genes in skeletal patterning and development. Development. 1997; 124:113–123. [PubMed: 9006072]

O'Gorman S, Dagenais NA, Qian M, Marchuk Y. Protamine-Cre recombinase transgenes efficiently recombine target sequences in the male germ line of mice, but not in embryonic stem cells. Proc Natl Acad Sci U S A. 1997; 94:14602–14607. [PubMed: 9405659]

Ocbina PJ, Anderson KV. Intraflagellar transport, cilia, and mammalian Hedgehog signaling: analysis in mouse embryonic fibroblasts. Dev Dyn. 2008; 237:2030–2038. [PubMed: 18488998]

Ocbina PJ, Eggenschwiler JT, Moskowitz I, Anderson KV. Complex interactions between genes controlling trafficking in primary cilia. Nat Genet. 2011; 43:547–553. [PubMed: 21552265]

Pazour GJ, Baker SA, Deane JA, Cole DG, Dickert BL, Rosenbaum JL, Witman GB, Besharse JC. The intraflagellar transport protein, IFT88, is essential for vertebrate photoreceptor assembly and maintenance. J Cell Biol. 2002; 157:103–113. [PubMed: 11916979]

Qin H, Wang Z, Diener D, Rosenbaum J. Intraflagellar transport protein 27 is a small G protein involved in cell-cycle control. Curr Biol. 2007; 17:193–202. [PubMed: 17276912]

Qin J, Lin Y, Norman RX, Ko HW, Eggenschwiler JT. Intraflagellar transport protein 122 antagonizes Sonic Hedgehog signaling and controls ciliary localization of pathway components. Proc Natl Acad Sci U S A. 2011; 108:1456–1461. [PubMed: 21209331]

Rohatgi R, Milenkovic L, Scott MP. Patched1 regulates hedgehog signaling at the primary cilium. Science. 2007; 317:372–376. [PubMed: 17641202]

Rosenbaum JL, Witman GB. Intraflagellar transport. Nat Rev Mol Cell Biol. 2002; 3:813–825. [PubMed: 12415299]

Rosenthal J, Mangal V, Walker D, Bennett M, Mohun TJ, Lo CW. Rapid high resolution three dimensional reconstruction of embryos with episcopic fluorescence image capture. Birth Defects Res C Embryo Today. 2004; 72:213–223. [PubMed: 15495188]

Skarnes WC, Rosen B, West AP, Koutsourakis M, Bushell W, Iyer V, Mujica AO, Thomas M, Harrow J, Cox T, et al. A conditional knockout resource for the genome-wide study of mouse gene function. Nature. 2011; 474:337–342. [PubMed: 21677750]

Tan SY, Rosenthal J, Zhao XQ, Francis RJ, Chatterjee B, Sabol SL, Linask KL, Bracero L, Connelly PS, Daniels MP, et al. Heterotaxy and complex structural heart defects in a mutant mouse model of primary ciliary dyskinesia. J Clin Invest. 2007; 117:3742–3752. [PubMed: 18037990]

Tobita K, Liu X, Lo CW. Imaging modalities to assess structural birth defects in mutant mouse models. Birth Defects Res C Embryo Today. 2010; 90:176–184. [PubMed: 20860057]

Tran PV, Haycraft CJ, Besschetnova TY, Turbe-Doan A, Stottmann RW, Herron BJ, Chesebro AL, Qiu H, Scherz PJ, Shah JV, et al. THM1 negatively modulates mouse sonic hedgehog signal transduction and affects retrograde intraflagellar transport in cilia. Nat Genet. 2008; 40:403–410. [PubMed: 18327258]

Tsukui T, Capdevila J, Tamura K, Ruiz-Lozano P, Rodriguez-Esteban C, Yonei-Tamura S, Magallon J, Chandraratna RA, Chien K, Blumberg B, et al. Multiple left-right asymmetry defects in Shh(−/−) mutant mice unveil a convergence of the shh and retinoic acid pathways in the control of Lefty-1. Proc Natl Acad Sci U S A. 1999; 96:11376–11381. [PubMed: 10500184]

Tsumaki N, Tanaka K, Arikawa-Hirasawa E, Nakase T, Kimura T, Thomas JT, Ochi T, Luyten FP, Yamada Y. Role of CDMP-1 in skeletal morphogenesis: promotion of mesenchymal cell recruitment and chondrocyte differentiation. J Cell Biol. 1999; 144:161–173. [PubMed: 9885252]

Tukachinsky H, Lopez LV, Salic A. A mechanism for vertebrate Hedgehog signaling: recruitment to cilia and dissociation of SuFu-Gli protein complexes. J Cell Biol. 2010; 191:415–428. [PubMed: 20956384]

Tuson M, He M, Anderson KV. Protein kinase A acts at the basal body of the primary cilium to prevent Gli2 activation and ventralization of the mouse neural tube. Development. 2011; 138:4921–4930. [PubMed: 22007132]

Wang Q, Pan J, Snell WJ. Intraflagellar transport particles participate directly in cilium-generated signaling in Chlamydomonas. Cell. 2006; 125:549–562. [PubMed: 16678098]

Wang Y, McMahon AP, Allen BL. Shifting paradigms in Hedgehog signaling. Curr Opin Cell Biol. 2007; 19:159–165. [PubMed: 17303409]

Wang Z, Fan ZC, Williamson SM, Qin H. Intraflagellar transport (IFT) protein IFT25 is a phosphoprotein component of IFT complex B and physically interacts with IFT27 in Chlamydomonas. PLoS One. 2009; 4:e5384. [PubMed: 19412537]

Wilson CW, Stainier DY. Vertebrate Hedgehog signaling: cilia rule. BMC Biol. 2010; 8:102. [PubMed: 20687907]

Highlights

- IFT25 is not required for cilia assembly
- *Ift25* mutant mice die at birth with Hedgehog dysfunction phenotypes
- *Ift25* mutant cells are defective in dynamic movements of signaling components

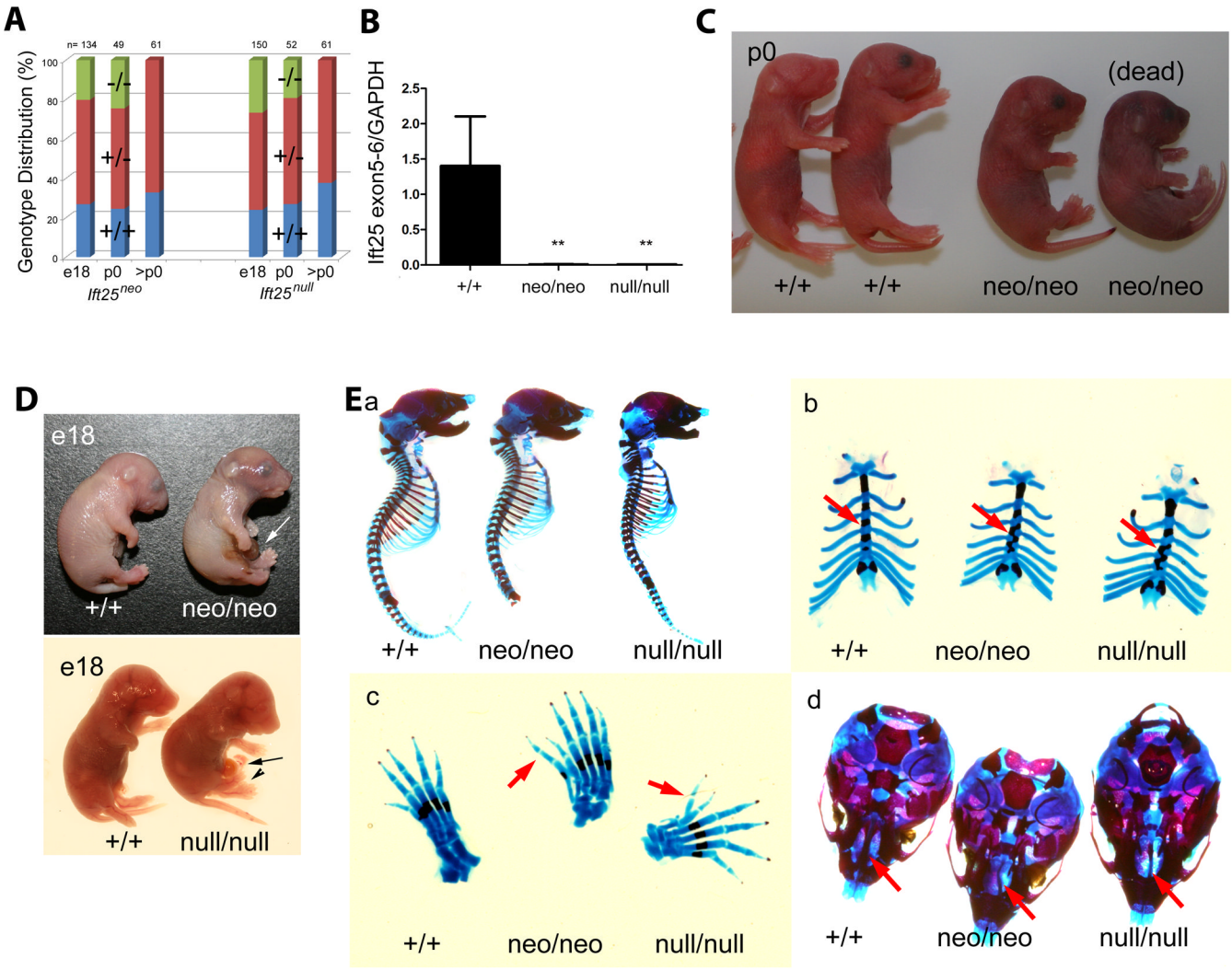

Figure 1. ***Ift25*** **null mutants display multiple developmental defects**

A. Genotype distribution at the day prior to birth (e18), day of birth (p0) and later (>p0) in offspring of $Ift25^{neo/+}$ by $Ift25^{neo/+}$ and $Ift25^{null/+}$ by $Ift25^{null/+}$ crosses. Blue, orange and green represent +/+, +/− and −/− genotypes respectively. Homozygous mutant animals were alive on the day prior to birth but died on p0 so the p0 numbers reflect a mix of live and dead animals. **B.** Quantitative PCR measurement of the level of *Ift25* mRNA in the two alleles (**p=.0028 for neo/neo and **p=.0078 for null/null). **C.** Images of p0 animals. Genotypes are given below. The three animals on the left were alive when photographed. **D.** Images of e18 embryos. Arrows denote omphaloceles and arrowhead denotes polydactyly. **E.** Alcian blue and alizarin red staining of the skeletons shows cranial abnormalities (**Ea**), malalignment of the sternal vertebrae (**Eb**), preaxial polydactyly (**Ec**) and cleft palate (**Ed**).

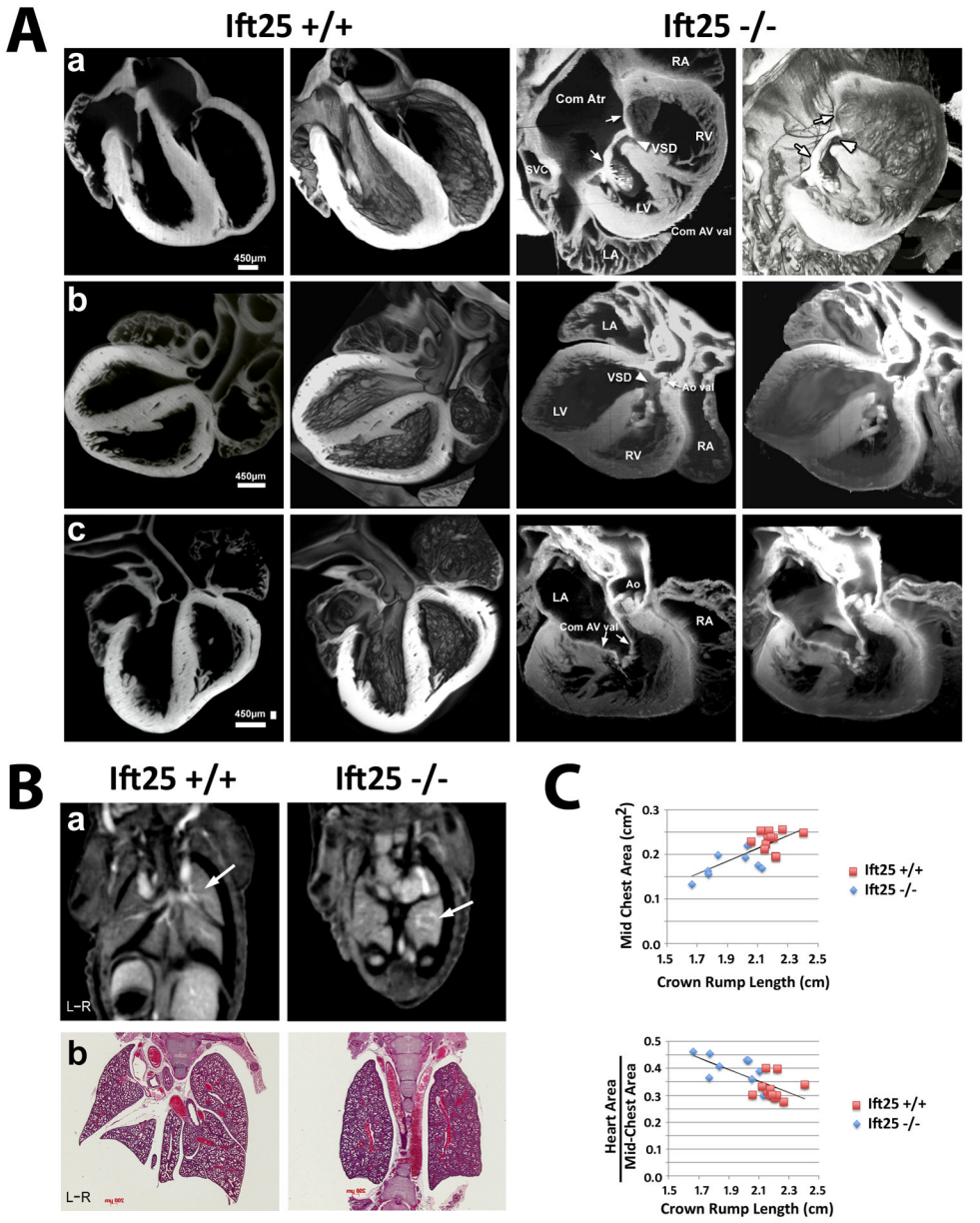

Figure 2. *Ift25* mutants have structural heart and lung disease

A. EFIC imaging of mutant hearts reveals structural heart defects. The two columns on the right are an *Ift25* mutant heart shown in 2-D view (left panels) and 3-D (right panels) renderings of movies included in the supplementary material. Panels on the left are of a control heart shown in similar 2D views and 3D renderings for comparison to the mutant heart images. **Aa.** Atrial septal defect causing a common atrium (Com Atr) with common atrioventricular valves (Com AV val) and an atrioventricular septal defect. The two white arrows point to the common AV valve and the arrowhead points to the VSD. **Ab.** Overriding aorta with membranous VSD. Note the aortic valve (Ao val) overrides the VSD (arrowhead). **Ac.** Common atrioventricular valves associated with an AVSD. This view shows the common AV valve (Com AV val) (arrows) as seen from the atrium. One common valve occupies the AV orifice instead of the normal right-sided tricuspid and left-sided mitral valves. Ao, aorta; SVC, left superior vena cava; LA, left atrium; RA, right atrium;

LV, left ventricle; RV, right ventricle. **B.** Lung isomerism. **Ba.** Single plane images from a microCT reconstruction of the thoracic cavity. *Ift25* controls show the multi-lobed lung (arrow) as expected whereas $Ift25^{neo/neo}$ animals have abnormal lobes (arrow). **Bb.** H&E images show the normal arrangement of 4 right lobes and 1 left lobe in the control animal but a single lobe on both sides in the mutant indicating a left isomerism. Some hypoplasia is noted in the H&E stained mutant lungs. **C.** MicroCT was used to measure the chest and heart cross sectional areas and the crown rump lengths in control (red squares) and mutant animals (blue diamonds). Note that mutants have reduced chest cross sectional areas ($p<0.001$) and reduced crown rump lengths ($p<0.001$) but their heart size is not different from controls ($p=0.35$).

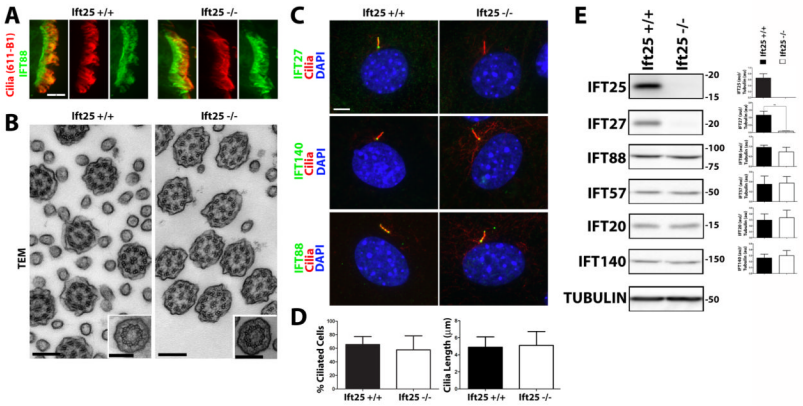

Figure 3. Unlike other complex B null mutants, *Ift25* null mutant cells are ciliated

A. e18.5 lung sections from *Ift25*$^{+/+}$ and *Ift25*$^{null1/null1}$ mice immunostained with IFT88 (green) and the acetylated tubulin cilia marker 611-B1 (red). Scale bar is 5μm and applies to all images. **B**. TEM analysis of e18.5 trachea cilia demonstrates no major differences between cilia of wild type and mutant littermates. Insets are images from the transition zone. Note that the slightly oval shape of the mutant cilia is likely a sectioning artifact since all cilia are compressed in the same direction. Scale bars = 0.2 μm. **C**. Immunofluorescence of control and null mutant MEFs immunostained with 611-B1 (Cilia, red) and IFT27, IFT88, or IFT140 (green). **D**. Quantitation of ciliation and ciliary length in MEF cells. Percentage of ciliated cells and ciliary lengths based on ciliary IFT88 immunostaining in serum starved MEFs (n=4 *Ift25*$^{+/+}$ and 6 *Ift25*$^{null1/null1}$ embryos for % ciliation and n=50 cilia per genotype for length). **E**. Effect of the *Ift25*^{null1} mutation on the IFT complex. Protein extracts from wild-type and homozygous null mutant MEFs were immunoblotted with the antibodies indicated on the left side of each western blot panel. Molecular weight markers are listed on the right side. Quantitation of IFT protein levels are listed on the right side of each western blot (n=3 embryos per genotype) (**p=0.0022).

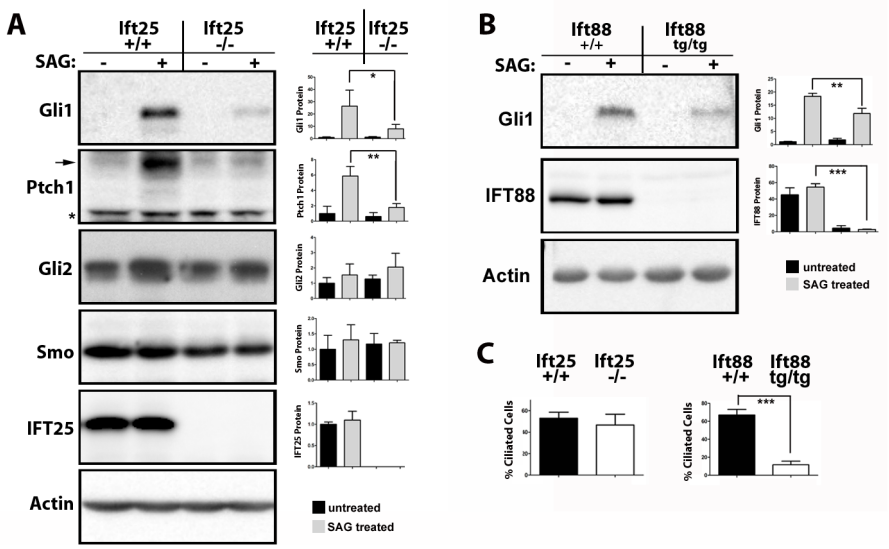

Figure 4. IFT25 is required for normal Hedgehog signaling response

A. *Ift25* $^{+/+}$and *Ift25*$^{null1/null1}$ MEFs were left untreated or treated with SAG, a Shh pathway activator. Cell homogenates were immunoblotted with the antibodies indicated on the left side of each panel. Quantitation of protein levels are listed on the right side of each western blot (n=3 embryos per genotype) (*p=0.0385 and **p=0.0062). **B.** *Ift88*$^{+/+}$ and *Ift88*$^{Tg737Rwp/Tg737Rpw}$ MEFs were treated the same as in A (**p=0.0078 and ***p≤.0001). **C.** Percentage of ciliated cells for each genotype was scored based on IFT88 immunostaining (***p=0.0002).

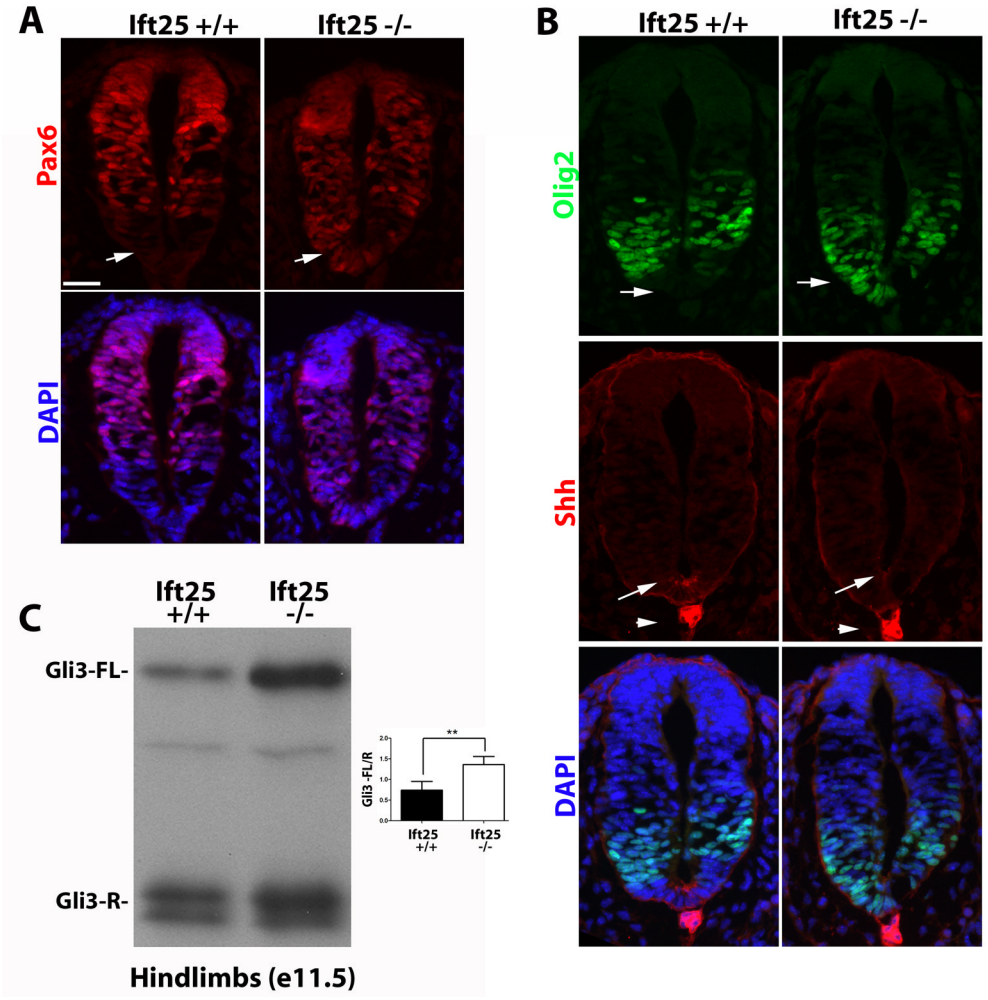

Figure 5. Hedgehog signaling is altered in the neural tube and limb buds of *Ift25* mutants

A. Neural tube patterning of *Ift25*$^{null1/null1}$ embryos. All images are shown with the ventral side (floor plate) on bottom. Cryosections from caudal regions of e9.5 embryos immunostained with Pax6 (red). Merged images with DAPI (blue) are shown below. Arrows depict the absence of Pax6 in the wild type floor plate and an expansion of Pax6 into the mutant floor plate. Scale bar is 50 μm and applies to all images in A and B. **B.** Cryosections from caudal regions of *Ift25*$^{+/+}$and *Ift25*$^{null1/null1}$ e9.5 embryos immunostained with Olig2 (green, top panels), Shh (red, middle panels) and merged images with DAPI (blue, bottom panels). Arrowheads indicate the notochords expressing Shh normally in both wild type and mutants. Arrows depict the presence of Shh producing cells in the wild type floor plate and a reduction of Shh producing cells in the mutant floor plate. **C.** *Ift25*$^{+/+}$and *Ift25*$^{null1/null1}$ protein extracts from e11.5 hindlimbs were immunoblotted for Gli3 protein (FL=full length and R=repressor). Quantitation of Gli3 protein levels (ratio of FL/R) from hindlimbs is shown on the right side of gel (n=5 embryos per genotype, **p=0.0014).

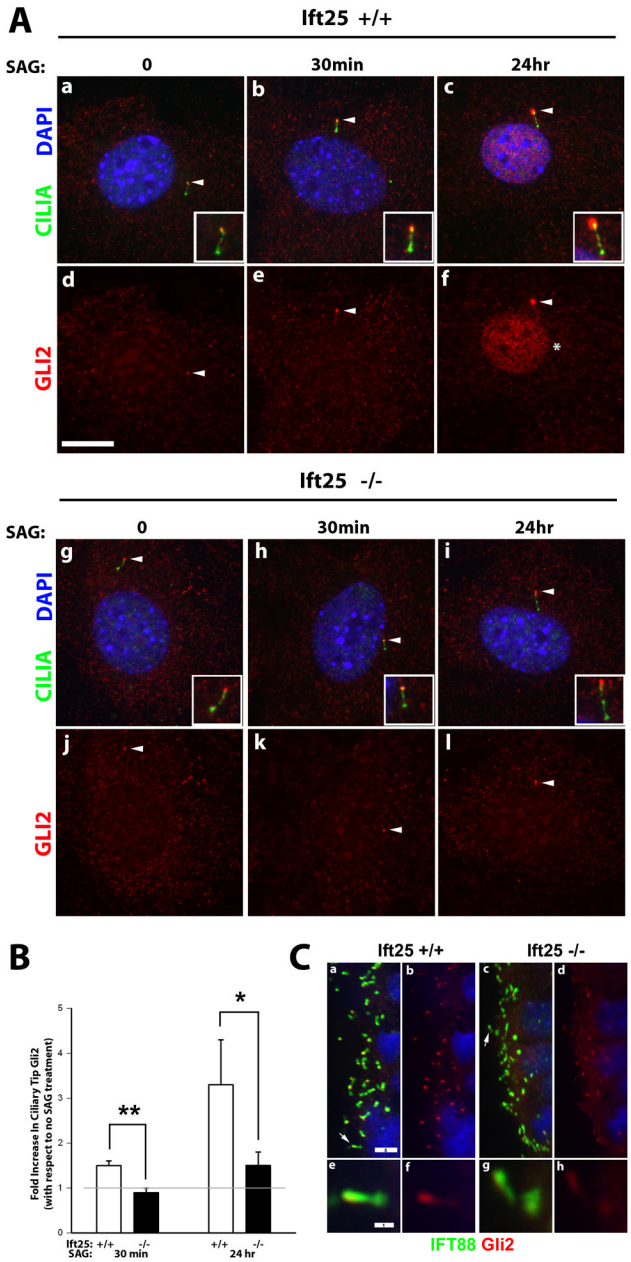

Figure 6. IFT25 is required for accumulation of Gli2 at ciliary tips in response to pathway activation

A. *Ift25*$^{+/+}$(a–f) and *Ift25*$^{null1/null1}$ MEFs (g–l) were treated with SAG for the indicated time points and immunostained with IFT88 to label cilia (green), Gli2 (red) and DAPI (blue). For *Ift25*$^{+/+}$ MEFs, the top row of panels (a–c) shows merged images and the bottom row of panels shows Gli2 only (d–f). For *Ift25*$^{null1/null1}$ MEFs, the top row of panels (g–i) shows merged images and the bottom row of panels shows Gli2 only (j–l). Arrowheads point to Gli2 staining at ciliary tips and these cilia are further magnified in insets; *indicates the nuclear Gli2 signal that appears after 24 hour SAG treatment (f). Scale bar is 10 μm and applies to all images except the insets. **B**. Quantitation of Gli2 immunofluorescence intensity at ciliary tips in response to SAG treatment (30 minutes and 24 hrs treatment). (n=3 embryos [MEF lines] per genotype) (**p=0.0059 at 30 minutes and *p=0.0385 at 24 hr). **C.** Aberrant

Gli2 localization in cilia of *Ift25* mutant embryos. Neural tubes of e10.5 $Ift25^{+/+}$ and $Ift25^{null1/null1}$ embryos immunostained for IFT88 (green) and Gli2 (red). Scale bar in panel **a** is 5 μm and applies to all four panels in the top row. Bottom row of panels are magnified images of the cilia that are highlighted with arrows from top panel. Scale bar in panel **e** is 1 μm and applies to all four panels in bottom row.

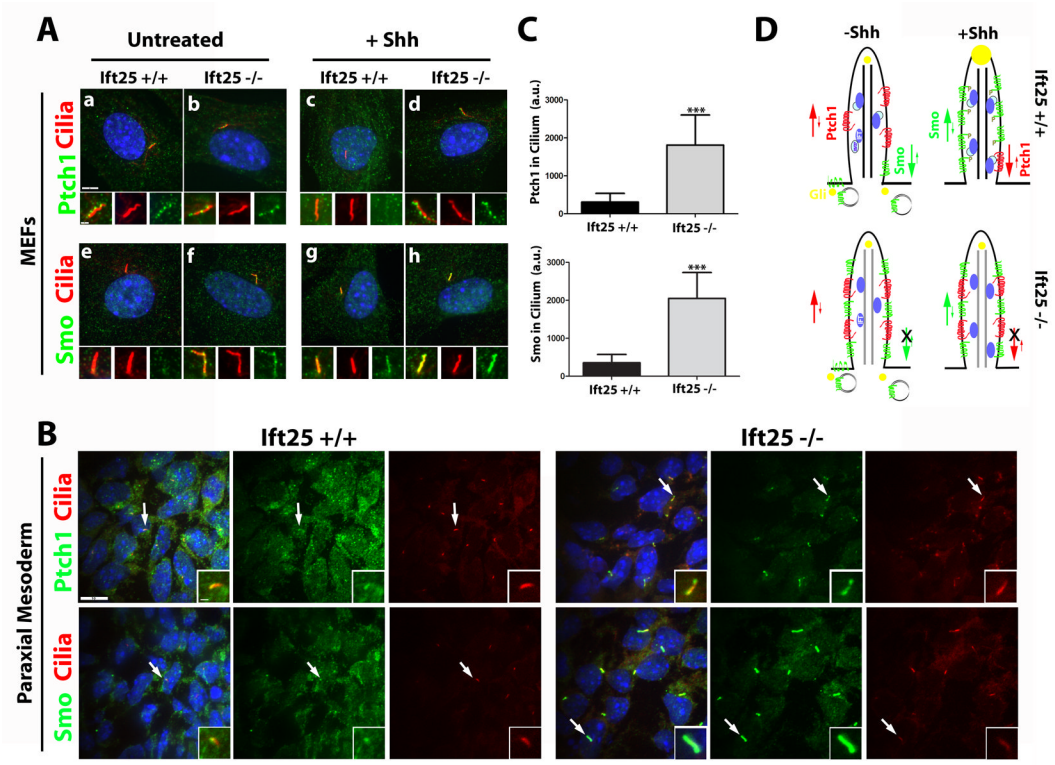

Figure 7. Ciliary export of Smo and Ptch1 is defective in *Ift25* mutants

A. *Ift25*$^{+/+}$ and *Ift25*$^{null1/null1}$ MEFs were untreated or treated with Shh for 4 hrs and immunostained for Ptch1 (green) in the top row of panels (a–d) or Smo (green) in the bottom row of panels (e–h). Cilia are stained with 611-B1 (red) and nuclei are stained with DAPI (blue) (a–h). Scale bar in panel a is 5 μm and applies to panels a–h. Magnified insets of cilia are shown underneath each corresponding panel with the scale bar representing 1 μm. Note that Smo is aberrantly present in untreated *Ift25* mutant cilia and Ptch1 is not exported from the cilium after Shh treatment. **B.** *Ift25* mutant embryos have elevated Smo and Ptch1 in cilia. Paraxial mesoderm regions of e10.5 embryo cryosections immunostained with Ptch1 (green) in the top row of panels and Smo (green) in the bottom row of panels. Cilia are stained with 611-B1 (red) and nuclei are stained with DAPI (blue). Scale bar is 10 μm and applies to all panels except insets. Arrows point to cilia that are further magnified in the insets. Scale bar in first inset is 1μm and applies to all insets. Note the elevations of both Ptch1 and Smo in the cilia of *Ift25*$^{null1/null1}$ embryos. **C.** Quantitation of ciliary Smo and Ptch1. Fluorescence intensity of Smo and Ptch1 in the paraxial mesoderm cilia was quantitated from three embryos per genotype (20 cilia each) (***p<0.0001). **D.** Model of IFT25 function in Hedgehog signaling. Ptch1 and Smo likely cycle continuously in and out of the cilium with a regulated export mechanism such that under basal conditions, Ptch1 is retained in the cilium and Smo is removed. After pathway activation (+Shh), the reverse occurs so Ptch1 is removed and Smo accumulates. Gli2 is normally present at the ciliary tip under basal conditions, but accumulates there after activation. In the absence of IFT25, the remaining IFT particle still assembles cilia but these cilia show an abnormal accumulation of Smo in the basal state. After pathway activation, *Ift25* mutants fail to export ciliary Ptch1 and fail to accumulate Gli2 at the ciliary tip. Thus, we propose that IFT25 functions to couple these dynamic movements to the IFT system.